Special Issue

Enhanced-Depth Imaging Optical Coherence Tomography of the Human Choroid In Vivo Compared With Histology After Enucleation

Xiao Qiang Li,[1,2] Steffen Heegaard,[1,2] Jens Folke Kiilgaard,[1,2] Inger Christine Munch,[2,3] and Michael Larsen[1,2]

[1]Department of Ophthalmology, Rigshospitalet, Copenhagen, Denmark
[2]Faculty of Health and Medical Sciences, University of Copenhagen, Copenhagen, Denmark
[3]Department of Ophthalmology, Zealand University Hospital, Roskilde, Denmark

Correspondence: Xiao Qiang Li, Rigshospitalet - Glostrup, Nordre Rinvej 57, 2600 Glostrup, Denmark; xiao.qiang.li@regionh.dk.

Submitted: December 13, 2015
Accepted: May 9, 2016

Citation: Li XQ, Heegaard S, Kiilgaard JF, Munch IC, Larsen M. Enhanced-depth imaging optical coherence tomography of the human choroid in vivo compared with histology after enucleation. *Invest Ophthalmol Vis Sci*. 2016;57:OCT371–OCT376. DOI:10.1167/iovs.15-18884

Purpose. This study compared in vivo enhanced-depth imaging optical coherence tomography (EDI-OCT) with ex vivo histology of the choroid in human eyes.

Methods. Three eyes in three patients with advanced iris melanoma without posterior segment involvement underwent EDI-OCT less than 24 hours prior to enucleation and, in one eye, immediately after enucleation. Following fixation in 4% buffered formaldehyde and paraffin embedding, serial sections of the whole eye were cut horizontally, mounted, stained with hematoxylin-eosin and digitized. Alignment between histology and EDI-OCT was made on landmarks such as retinal vessel, the foveal depression, ciliary arteries, drusen, and nevi.

Results. Intra- and interindividual variations in relative choroidal thickness were comparable between the two modalities. After histologic fixation of the three melanoma eyes, the fullness of the choroidal vessels was reduced and subfoveal choroid thickness reduced to 56%, 45%, and 56%, respectively, of its in vivo thickness on EDI-OCT.

Conclusions. There were no identifiable discrepancies in choroidal structural patterns between clinical EDI-OCT and histologic sections except that after enucleation and histologic fixation choroidal thickness was reduced to roughly half of its in vivo value, a phenomenon that may reflect the high content of blood vessels in the choroid.

Keywords: choroid, EDI-OCT, histology

Enhanced-depth imaging optical coherence tomography (EDI-OCT) and swept-source optical coherence tomography (SS-OCT) have enabled in vivo visualization of the choroid at high resolution and deep penetration[1] and shown that various observations made on histologic samples, such that of an age-related attenuation of choroid thickness, can be replicated in vivo.[2,3] Previous in vivo studies of human choroidal anatomy based on EDI-OCT have described variations in thickness, structure, and volume in relation to age, disease, and therapy in age-related macular degeneration and central serous chorioretinopathy[1,4] and have addressed structural details such as the visibility of the border between Sattler's and Haller's layers and presence of a suprachoroidal space.[5–7]

This report describes the relation between the choroidal morphology and thickness on EDI-OCT in vivo and on corresponding histologic sections from the same eyes made after enucleation because of iris melanoma.

Patients and Methods

This retrospective observational study comprised three eyes with intractable iris melanoma in three patients (two females, one male; Table 1). The study was conducted according to the Declaration of Helsinki. Clinical procedures, including a standard ophthalmic examination and OCT (Spectralis HRA-OCT; Heidelberg Engineering, Heidelberg, Germany), were made within 24 hours before enucleation. In all three patients, ocular imaging included a 30 × 5 degree fovea-centered EDI-OCT field covered by 49 horizontal B scans spaced 30 μm apart. In patient no. 3, EDI-OCT also included two 30 × 25–degree EDI-OCT with 121 horizontal B scans set at 61-μm intervals and centered on the fovea and on the optic nerve head, respectively. Postenucleative EDI-OCT was performed in one patient (patient no. 3) immediately after enucleation while the cornea was still clear. The eye was held manually in front of the scanning laser ophthalmoscope, and by using the instrument's active eye tracking system (TruTrack TM; Heidelberg Engineering) it was possible to obtain retinal scans aligned to preenucleated scans of the same eye.

Choroidal thickness on EDI-OCT was measured manually by one of the authors (XQL) using the instrument manufacturer's proprietary software (Heidelberg Explorer 1.7.1.0; Heidelberg Engineering) as previously described.[8] The suprachoroidal space was identified on the EDI-OCT as a hyper-hypo-hyper-reflective band of relatively uniform thickness separating the choroid and the sclera and being visible on consecutive scans.[6] Lateral magnification was adjusted according to the refractive characteristics of the individual eyes.

After enucleation, the eyes were fixed in 4% buffered formaldehyde for more than 24 hours and subsequently embedded in paraffin. Multiple parallel, horizontal 5-μm-thick

Table 1. Clinical Characteristics of the Study Subjects

	Patient 1	Patient 2	Patient 3
Age/sex	74/female	56/male	72/female
Target eye	Right	Right	Left
Refractive error	−2.0 D	−2.0 D	−0.5 D
IOP, mm Hg	12	28	12
EDI to enucleation and fixation	20 h	14 h	20 h

D, diopter.

serial sections (160, 108, and 1000 sections from patients no. 1, no. 2, and no. 3, respectively) were cut from the posterior pole, including the optic nerve head, the temporal arcades, and the macula. The sections were mounted on glass slides and stained with hematoxylin-eosin and digitized in bright-field mode (Zeiss Axio Scan Z1; Carl Zeiss Microscopy GmbH, Jena, Germany) and viewed using proprietary display software (ZEN Blue 2012; Carl Zeiss Microscopy GmbH).

Histology sections and EDI-OCT scans were evaluated for alignment and skewedness by visual identification of landmarks such as blood vessels on the optic nerve head (Fig. 1) using the method previously described by Lassota and colleagues.[9] Other landmarks included the foveal depression (Fig. 2), posterior ciliary artery segments embedded in the sclera (Fig. 3), and solitary drusen and nevi (Table 2). On histology sections the suprachoroidal space was assumed to be present, as a potential or real space, at the transition between choroidal tissue, with its vessels and melanocytes, and in the ordered layers of collagen of the sclera.

Choroidal thickness was measured on matching EDI-OCT scans and histology sections every 100 μm and averaged over 1000 μm under the fovea and over 500 μm at selected extrafoveal locations. Corresponding thickness measurements in patient no. 1 were confined to the fovea because alignment was uncertain outside the fovea. Locations where artifacts such as choroidal detachment had occurred during preparation of the histologic sections were excluded from analysis.

Results

The angular offset between the EDI-OCT scans and the histology sections was 40 degrees in patient no. 1, less than 10 degrees in patient no. 2, and 15 degrees in patient no. 3 (Fig. 1).

In patient no. 1, subfoveal choroidal thickness was 176 μm on EDI-OCT compared with 98 μm (56%) on the corresponding histologic tissue section. In patient no. 2, the corresponding values were 239 μm and 108 μm (45%), and in patient no. 3 they were 308 μm and 174 μm (56%; Table 3), respectively. In patients no. 2 and no. 3, the choroidal thickness values measured 3 mm from the fovea on histologic sections were between 47% and 60% of the EDI-OCT values (Table 3). The reduction in choroidal thickness between in vivo and ex vivo examinations was uniform over the posterior pole of the eye, showing a comparable extrafoveal-to-subfoveal choroidal thickness ratio on both EDI-OCT and in histology (Table 3: patients no. 2 and no. 3).

In all three patients, large choroidal arteries continuous with long posterior ciliary arteries could be matched on EDI-OCT and histologic sections (Fig. 3).

A suprachoroidal space was visible on EDI-OCT only in patient no. 3 most distinctly under the macula, but the histology sections showed only heavy pigmentation without any tissue cleft at the corresponding location along with posterior ciliary arteries (Fig. 3C; Supplementary Video).

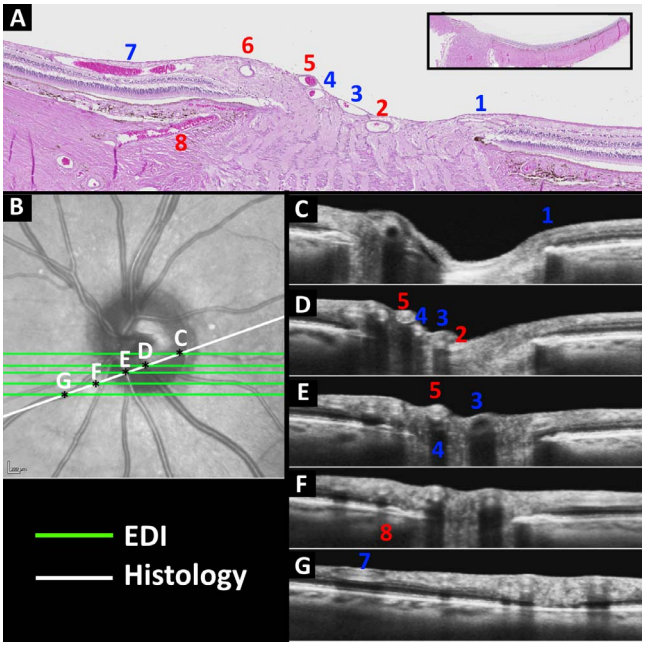

Figure 1. Comparison of histologic section (**A**), infrared fundus photography with EDI-OCT section line (**B**), and EDI-OCT scans in 1:1 μm (labels also referring to points of intersection between OCT and histology sections) (**C–G**) from the right eye of patient no. 3. Landmark features include retinal veins (1, 3, 4, and 7; *blue*), retinal arteries (2, 5, and 6; *red*), and a transscleral ciliary artery (8; *red*) that were unique to their location. Analysis of serial EDI scans (**C–G**) showed that the histology section (**A**) was skewed in relation to the EDI-OCT scans by an angle of approximately 15 degrees.

The immediate postenucleation EDI-OCT made in patient no. 3 showed that the retinal and choroidal vessels had partially collapsed and that the normal tri-layer reflectivity of the flowing blood in the retinal vessels had disappeared (Fig. 4). On the immediate postenucleation EDI-OCT, the subfoveal choroidal thickness was 82% of the preenucleation thickness (Table 3).

Discussion

Comparison of in vivo EDI-OCT with ex vivo postenucleation histology sections demonstrated a high degree of consistency between the structural features of the choroid, whereas the absolute thickness of the choroid had been reduced on histologic sections to approximately 50% of its in vivo value. Prominent landmarks such as ciliary arteries passing through the sclera could be identified on both modalities, which enabled a convincing alignment of sections from the two imaging modalities. Immediate postenucleative EDI-OCT showed retinal vessel deflation and modest choroidal thickness decrease.

The accuracy of choroidal thickness measurements is limited by the ability to define the choroidoscleral border, especially on EDI-OCT. The assessment of relative change in thickness is facilitated, however, by the ability to see a shift in the whole framework of choroidal structures, a phenomenon that is best seen when toggling between aligned images with highlighted landmarks. Previous studies comparing histology with OCT in human eyes used OCT instruments that cannot

Investigative Ophthalmology & Visual Science

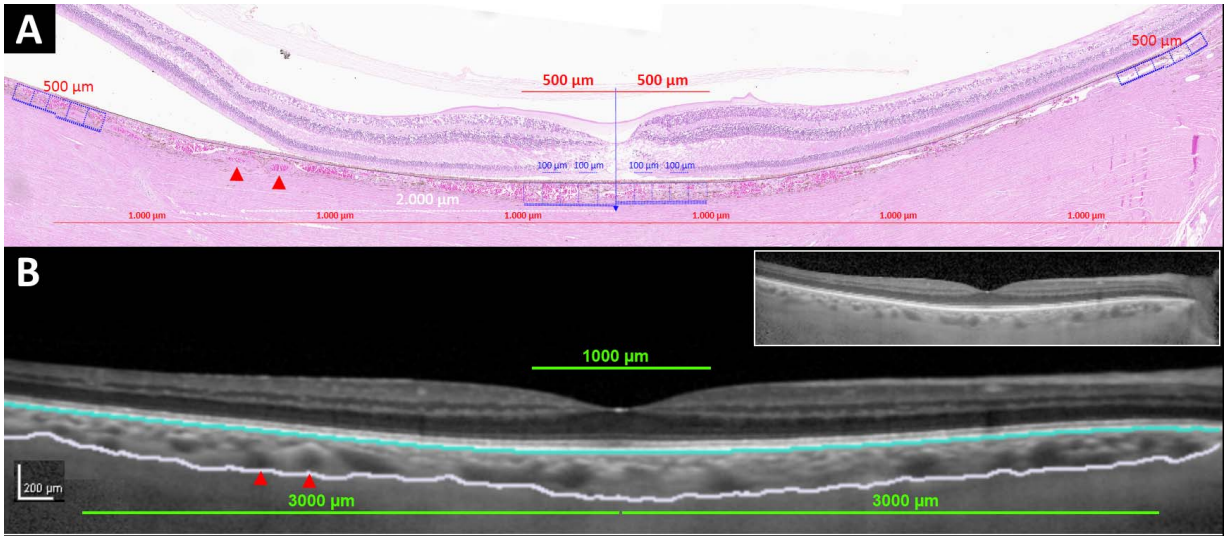

FIGURE 2. Horizontal transfoveal sections through the right eye of patient no. 2 comparing a histologic preparation (**A**) with enhanced OCT (**B**). Choroidal thickness was averaged over 1000 µm under the fovea and over 500 µm at distances of 3 mm on the nasal and 3 mm on the temporal side of the fovea (*blue lines*). Two large arteries of the outer choroid seen in both modalities (*red arrowheads*) show the change in vessel lumen diameter after enucleation. Bruch's membrane (*cyan*) and the choroidoscleral border (*white*) are marked on (**B**). A retinal detachment (*left*) (**A**) was only seen after histologic preparation, as is the case in the following figures.

image the entire choroid,[10] or used only ex vivo OCT, or used different eyes for OCT and histology sections,[11,12] or used animal eyes.[13–17] This review of cases is, to the best of our knowledge, the first study to compare the choroid in in vivo EDI-OCT with ex vivo histology in the same eyes in humans.

Studies of choroidal histology have found subfoveal choroidal thickness values of typically 200 µm at birth, with a gradual decrease with age.[3] The present study reconciles these results with those made using EDI-OCT studies in recent years, which have found a wide range of variation and average values of typically 300 µm.[1]

Comparative studies of retinal thickness on OCT and on histologic sections have also found evidence of some shrinkage during tissue preparation,[12] but not to the extent seen for the choroid in the present study. The difference appears to be that the choroid has a far larger vascular component than does the retina. The spatial variability of choroidal thickness was comparable on EDI-OCT and histology sections, the choroid being thickest under the fovea, thinner temporal of the fovea, and thinnest nasal of the fovea.[1]

Choroidal thickness on EDI-OCT is usually defined as the distance between the well-defined Bruch's membrane and the outer aspect of the choroid. The latter is more difficult to define due to the decreasing signal-to-noise ratio on OCT with increasing scanning depth, the presence of choroidal melanocytes, and the irregular morphology of the outer choroid. The choroidal/scleral border is more difficult to define where the posterior ciliary arteries penetrated the sclera.[6,18]

A suprachoroidal space was visible on EDI-OCT in one out of the three eyes and had disappeared on histology sections, which suggests that this structure may also be maintained by hydrostatic pressure gradients and fluid movement inside the eye and the orbit. The suprachoroid is classically defined as a 30-µm-thick[19] interface between the choroid and the sclera

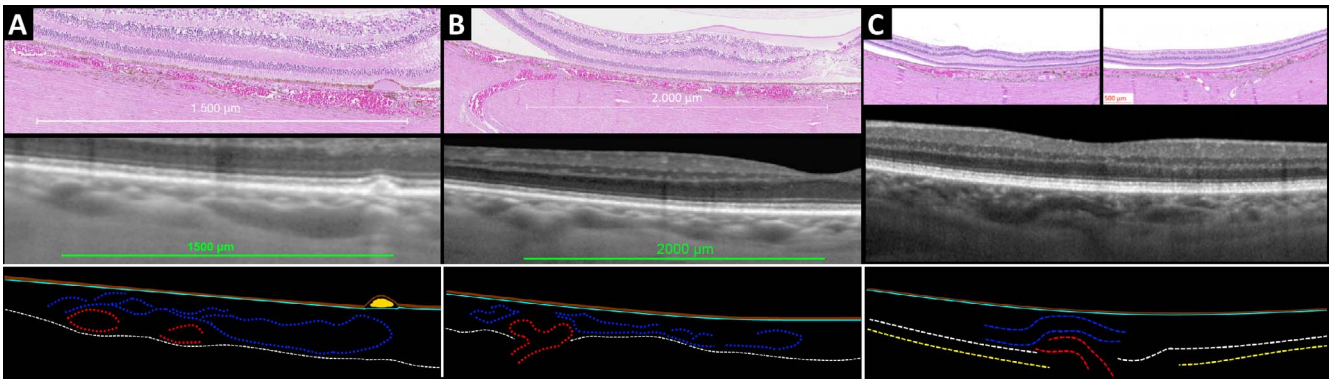

FIGURE 3. Histologic sections and enhanced OCT scans aligned on landmarks such as a solitary druse (**A**) and ciliary arteries near or within the sclera (**B**, **C**). Outline sketches show the retinal pigment epithelium (*brown*), its basal membrane (*cyan*), choroidal/ciliary arteries (*red*), choroidal veins (*blue*), drusen (*yellow*), and the choroidoscleral border (*white*). A suprachoroidal space seen on EDI-OCT in patient no. 3 (*white* and *yellow stippled outline*) (**C**) is not apparent on the histologic section, whereas an adjacent section/scan pair shows a characteristic ciliary artery. For more detail, please see the Supplementary Material.

Investigative Ophthalmology & Visual Science

Table 2. Matching Landmarks Between EDU-OCT and Histology

	Patient 1	Patient 2	Patient 3
Foveal centration	Yes	Yes	Yes
Optic nerve head border and serial peripapillary retinal vessel orientation	Yes	Yes	Yes
Unique juxtachoroidal landmarks	• Subfoveal posterior ciliary artery insertion	• Juxtafoveal solitary drusen • Temporal transscleral ciliary artery emissaries	• Juxtapapillary drusen • Temporal transscleral short ciliary artery • Large choroidal vessels • Choroidal nevus

that forms a potential space in healthy eyes, limited externally by the lamina fusca.[6,7,20,21] Using EDI-OCT, Yiu et al. found a visible suprachoroid in nearly half of 74 healthy controls aged 55 to 85 years from the Age-Related Eye Disease Study 2 .[7] With SS-OCT, Michalewska et al. found a suprachoroidal space in only 5% of healthy subjects.[6] It thus appears that methodologic factors affect the results.

Immediate postenucleation EDI-OCT was available for one enucleated eye. It showed that the retinal vessels were partially deflated and had lost the layered reflectivity pattern characteristic of flowing blood.[22,23] We also observed a reduction in choroidal thickness as an immediate effect of enucleation. The bulk of the reduction in choroidal thickness, however, was seen on the histologic sections after tissue processing. Thus, the difference in choroidal thickness between EDI-OCT in vivo and histology sections may be a result not only of exsanguination of the eye during the surgical procedure but also a result of the later stages in the processing of the tissue.

The transition between the medium-sized vessels of Sattler's layer and the large-sized vessels of Haller's layer was not prominent in the histology nor on EDI-OCT in this study. The Sattler's and Haller's layers are clearly better appreciated in en face in vivo imaging of the choroid, which shows the vascular pattern with authentic vessel diameters over a wider area of the choroid than can be seen in transverse sections.[24] A grading of Sattler's and Haller's layers on EDI-OCT was not included in this study.

The main limitation of the present study is its small sample size and the lack of extremes in choroidal thickness variation. Additionally, there was some rotational misalignment, which could be reduced in future studies by including a wider range of preenucleation scan orientations. Histologic artifacts were found, especially in the fovea. The choroid, however, was less prone to artifacts such as detachments. Skewed z-plane orientation was not evident but may have missed detection. A strength of the study includes the use of averaged choroidal thicknesses instead of single measurements that are more prone to variation. Secondly, the choroidal/scleral border on EDI-OCT was measured using methods with high inter- and intraoperator comparability and repeatability.[25,26] The size of the one solitary drusen (Fig. 3A) showed remarkable similarity between EDI-OCT and histology, supporting that our measurements on EDI-OCT were accurate. Lastly, we found a comparable range of shrinkage in all three eyes in both subfoveal and extrafoveal area. Taken together, we speculate that the choroidal thickness reduction by half was due to true tissue shrinkage rather than measurement error. However, despite comparable reduction of the absolute choroidal thickness in all three eyes in histology, results may remain tentative due to the limited sample size.

Table 3. Choroidal Thickness on EDI-OCT and Histology in Three Eyes Enucleated for Iris Melanoma

	EDI, mean; μm	Histology, mean; μm	Histology/EDI, %
Patient 1*			
Subfoveal	176	98	56
Patient 2			
Subfoveal	239	108	45
3 mm Nasal of fovea	147	69	47
3 mm Temporal of fovea	176	91	52
Nasal/subfoveal ratio	0.62	0.64	104
Temporal/subfoveal ratio	0.74	0.84	114
Patient 3†			
Subfoveal	308	174	56
3 mm Nasal of fovea	136	79	58
3 mm Temporal of fovea	191	115	60
Nasal/subfoveal	0.44	0.45	103
Temporal/subfoveal	0.62	0.66	107
Under drusen preenucleation	122	–	–
Under drusen postenucleation	101	–	–

* Extrafoveal measurements were not reported for patient no. 1 because of large angular misalignment between the two examination modalities.
† Subfoveal choroidal thickness and the choroid under drusen (patient no. 3) were measured at intervals of 100 μm and averaged over 1000 μm. Extrafoveal choroidal thickness was averaged over 500 μm.

Investigative Ophthalmology & Visual Science

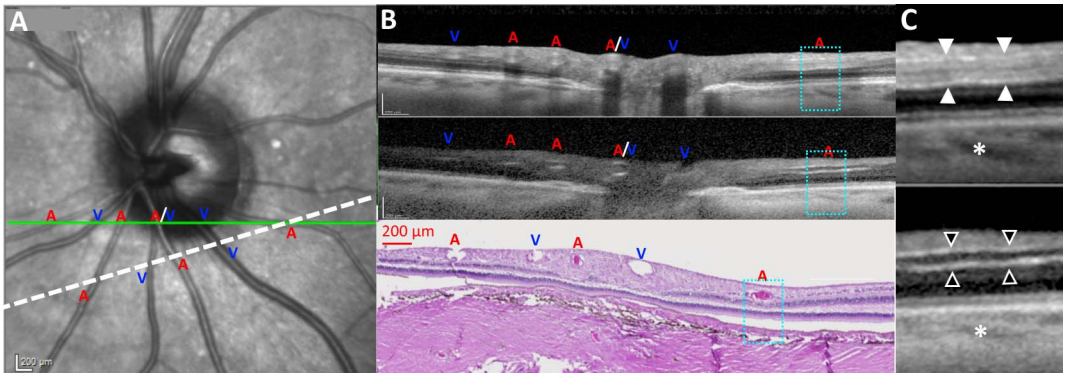

FIGURE 4. Infrared image (**A**) and EDI-OCT scans of the left eye of patient no. 3 recorded in vivo before (**B** [*top*; corresponds to *green line* on the infrared image], **C** [*top*; magnification of section marked by *dotted blue line* in **B**]) and ex vivo after enucleation (**B** [*middle*], **C** [*bottom*]). A near-parallel histology section shows matching retinal vessels (*bottom*; corresponds to *white broken line* on the infrared image) (**B**). After enucleation, the scan quality had deteriorated, and the internal reflectivity pattern characteristic of flowing blood (*top*; *white arrowheads*) (**C**) had disappeared (*bottom*; *black arrowheads*) and the retinal vessel diameters were reduced. A minor reduction in choroidal thickness was also visible (*asterisk*) (**C**).

In conclusion, our results support the common interpretation of choroidal morphology on EDI-OCT scans. The appearance of choroidal structures corresponded between EDI-OCT and histologic sections; however, choroidal thickness ex vivo was only half of that in vivo, supporting that the choroid is an elastic tissue that is kept inflated partly by the transmural pressure gradient across its vessel walls.

Acknowledgments

Supported by The Bagenkop Nielsen Myopia Foundation (Copenhagen, Denmark).

Disclosure: **X.Q. Li**, None; **S. Heegaard**, None; **J.F. Kiilgaard**, None; **I.C. Munch**, None; **M. Larsen**, None

References

1. Mrejen S, Spaide RF. Optical coherence tomography: imaging of the choroid and beyond. *Surv Ophthalmol*. 2013;58:387–429.
2. Spaide RF. Age-related choroidal atrophy. *Am J Ophthalmol*. 2009;147:801–810.
3. Ramrattan RS, van der Schaft TL, Mooy CM, de Bruijn WC, Mulder PG, de Jong PT. Morphometric analysis of Bruch's membrane, the choriocapillaris, and the choroid in aging. *Invest Ophthalmol Vis Sci*. 1994;35:2857–2864.
4. Imamura Y, Fujiwara T, Margolis R, Spaide RF. Enhanced depth imaging optical coherence tomography of the choroid in central serous chorioretinopathy. *Retina*. 2009;29:1469–1473.
5. Esmaeelpour M, Kajic V, Zabihian B, et al. Choroidal Haller's and Sattler's layer thickness measurement using 3-dimensional 1060-nm optical coherence tomography. *PLoS One*. 2014;9:e99690.
6. Michalewska Z, Michalewski J, Nawrocka Z, Dulczewska-Cichecka K, Nawrocki J. Suprachoroidal layer and suprachoroidal space delineating the outer margin of the choroid in swept-source optical coherence tomography. *Retina*. 2015;35:244–249.
7. Yiu G, Pecen P, Sarin N, et al. Characterization of the choroid-scleral junction and suprachoroidal layer in healthy individuals on enhanced-depth imaging optical coherence tomography. *JAMA Ophthalmol*. 2014;132:174–181.
8. Li XQ, Larsen M, Munch IC. Subfoveal choroidal thickness in relation to sex and axial length in 93 Danish university students. *Invest Ophthalmol Vis Sci*. 2011;52:8438–8441.
9. Lassota N, Kiilgaard JF, Prause JU, la Cour M. Correlation between clinical and histological features in a pig model of choroidal neovascularization. *Graefes Arch Clin Exp Ophthalmol*. 2006;244:394–398.
10. Chen TC, Cense B, Miller JW, et al. Histologic correlation of in vivo optical coherence tomography images of the human retina. *Am J Ophthalmol*. 2006;141:1165–1168.
11. Brown NH, Koreishi AF, McCall M, Izatt JA, Rickman CB, Toth CA. Developing SDOCT to assess donor human eyes prior to tissue sectioning for research. *Graefes Arch Clin Exp Ophthalmol*. 2009;247:1069–1080.
12. Curcio CA, Messinger JD, Sloan KR, Mitra A, McGwin G, Spaide RF. Human chorioretinal layer thicknesses measured in macula-wide, high-resolution histologic sections. *Invest Ophthalmol Vis Sci*. 2011;52:3943–3954.
13. McLellan GJ, Rasmussen CA. Optical coherence tomography for the evaluation of retinal and optic nerve morphology in animal subjects: practical considerations. *Vet Ophthalmol*. 2012;15(suppl 2):13–28.
14. Huang Y, Cideciyan AV, Papastergiou GI, et al. Relation of optical coherence tomography to microanatomy in normal and rd chickens. *Invest Ophthalmol Vis Sci*. 1998;39:2405–2416.
15. Gloesmann M, Hermann B, Schubert C, Sattmann H, Ahnelt PK, Drexler W. Histologic correlation of pig retina radial stratification with ultrahigh-resolution optical coherence tomography. *Invest Ophthalmol Vis Sci*. 2003;44:1696–1703.
16. Abbott CJ, McBrien NA, Grunert U, Pianta MJ. Relationship of the optical coherence tomography signal to underlying retinal histology in the tree shrew (*Tupaia belangeri*). *Invest Ophthalmol Vis Sci*. 2009;50:414–423.
17. Strouthidis NG, Grimm J, Williams GA, Cull GA, Wilson DJ, Burgoyne CF. A comparison of optic nerve head morphology viewed by spectral domain optical coherence tomography and by serial histology. *Invest Ophthalmol Vis Sci*. 2010;51:1464–1474.
18. Ruiz-Medrano J, Flores-Moreno I, Pena-Garcia P, Montero JA, Duker JS, Ruiz-Moreno JM. Asymmetry in macular choroidal thickness profile between both eyes in a healthy population measured by swept-source optical coherence tomography. *Retina*. 2015;35:2067–2073.

19. Hogan M. Choroid. In: *Histology of the Human Eye*. Philadelphia, PA: W.B. Saunders Company; 1971:321.
20. Lumbroso B, Rispoli M. Basic normal anatomy and OCT. In: *Practical Handbook of OCT*. India: Jaypee Brothers; 2012:15.
21. Kiilgaard J, Jensen P. The choroid and the optic nerve head. In: Fischbarg J, ed. *The Biology of the Eye*. London: Elsevier; 2005: 406.
22. Muraoka Y, Tsujikawa A, Murakami T, et al. Morphologic and functional changes in retinal vessels associated with branch retinal vein occlusion. *Ophthalmology*. 2013;120:91–99.
23. Willerslev A, Li XQ, Cordtz P, Munch IC, Larsen M. Retinal and choroidal intravascular spectral-domain optical coherence tomography. *Acta Ophthalmol*. 2014;92:126–132.
24. Branchini LA, Adhi M, Regatieri CV, et al. Analysis of choroidal morphologic features and vasculature in healthy eyes using spectral-domain optical coherence tomography. *Ophthalmology*. 2013;120:1901–1908.
25. Shao L, Xu L, Chen CX, et al. Reproducibility of subfoveal choroidal thickness measurements with enhanced depth imaging by spectral-domain optical coherence tomography. *Invest Ophthalmol Vis Sci*. 2013;54:230–233.
26. Li XQ, Munkholm A, Larsen M, Munch IC. Choroidal thickness in relation to birth parameters in 11–12 year-old children: The Copenhagen Child Cohort 2000 Eye Study. *Invest Ophthalmol Vis Sci.*. 2015;56:617–624.

Investigative Ophthalmology & Visual Science